

## **Abstract**

In situations where daylight is insufficiently available, Virtual Natural Lighting Solutions (VNLS) can be promising to turn currently unused floor space into spaces with enough daylight qualities. This article introduces VNLS models with complex image scenes pasted on a transparent glass surface in front of arrays of small, directional white light sources. The objectives are twofold; the first one is to understand the effect of changing input variables, i.e. beam angle, total luminous flux of the ‘sky’ elements, and image scene itself; on the lighting performance of a reference office space. The second objective is to compare two techniques of modelling the view, i.e. transmissive and emissive approaches, using *Radiance*. Sensitivity analysis of the simulation results show that under every image scene, the total luminous flux of the ‘sky’ element is largely influential to the space availability, whereas the beam angle of the ‘sky’ element is largely influential to the other output variables, including discomfort glare. The findings lead to a suggestion of preferred elements in the image scene, to ensure large space availability and uniformity. The transmissive approach generally generates smaller values of space availability, and largely depends on the view elements of the image scene. In turn, the average probability of discomfort glare using the transmissive approach is smaller than that using the emissive approach.

**Keywords:** virtual natural lighting solution, view, light, transmissive, emissive, simulation

## List of Symbols

### Roman symbols

$\%A$	space availability [%]
$\%G$	ground contribution on the ceiling [%]
$\%G_{av}$	average ground contribution on the ceiling [%]
BA	beam angle of the 'sky' element [°]
$n(E \geq 500 \text{ lx})$	number of points with illuminance $\geq 500 \text{ lx}$ [%]
DGP	daylight glare probability [-]
$DGI_n$	normalised daylight glare index [-]
DGI	daylight glare index [-]
CGI	CIE glare index [-]
$CGI_n$	normalised CIE glare index [-]
$E_{av}$	average illuminance [lx]
$E_{min}$	minimum illuminance [lx]
IA	interval of tilt angle of the 'sky' element [°]
$N$	total number of points [-]
$PDG_{av}$	average probability of discomfort glare [-]
$U_0$	uniformity [-]
UGR	unified glare rating [-]
$UGR_n$	normalised unified glare rating [-]

### Greek symbols

$\beta$	regression coefficient [-]
$\beta'$	standard regression coefficient [-]
$\rho$	weighted average spectral reflectance [-]
$\rho_R$	spectral reflectance in red [-]
$\rho_G$	spectral reflectance in green [-]
$\rho_B$	spectral reflectance in blue [-]
$\tau$	weighted average spectral transmittance [-]
$\tau_R$	spectral transmittance in red [-]
$\tau_G$	spectral transmittance in green [-]
$\tau_B$	spectral transmittance in blue [-]
$\Phi$	total luminous flux of the 'sky' element [lm]

## 1. Introduction

Many researchers have shown the benefit of daylight with regard to health and well-being, and that in general, people with sufficient access to daylight perceive less stress, have a higher productivity, and are more alert, e.g. (Heschong et al. 2002; Heschong 2003; Boyce et al. 2003). In cases where daylight is unavailable, for instance during nighttimes or in deeper parts of buildings, the Virtual Natural Lighting Solutions (VNLS) concept can be promising. VNLS are systems that can artificially provide natural lighting as well as a realistic outside view, with properties comparable to those of real windows and skylights. The benefit of installing VNLS in a building is the ability to use spaces which have very limited or no access to daylight, with the possibility to control the lighting and view quality.

The ideal VNLS product does not yet exist at the moment, but there is a need to predict how these future solutions will affect the performance of a given space in buildings. Since VNLS have lots of possible input variables, computational building performance simulation is required to predict their performance. In terms of lighting performance, we have employed *Radiance* (Ward and Shakespeare 1998) as the main tool to model the VNLS as arrays of small light sources constructing a simplified view that resembles the blue sky and green ground (Mangkuto et al. 2014). The blue-coloured ‘sky’ elements are tilted downward to deliver the majority of the light to the workplane, while the green-coloured ‘ground’ elements are tilted upward to deliver most of the light to the ceiling, referring to the ideal CIE overcast sky where the split-flux method applies (Tregenza 1989).

Sensitivity analysis was applied to evaluate the influence of four input parameters, i.e. total luminous flux of the ‘sky’ elements, interval of tilt angle, beam angle, and distance between windows; to the output parameters, i.e. space availability, uniformity, average ground contribution on the ceiling, and average probability of discomfort glare. The comparison with scenes with simulated real windows under the CIE overcast sky was also

presented. The results show that the total luminous flux greatly influences the space availability, while the beam angle is highly influential on the uniformity, average ground contribution on the ceiling, and average probability of discomfort glare. Most of the investigated VNLS that satisfy all criteria (in terms of ratio, compared to the real windows scene) are those having a beam angle of  $114^\circ$  (wide spread) (Mangkuto et al. 2014).

While the findings may give an illustration on how VNLS will perform in a space, it is noticed that VNLS ideally should generate a directional (non-diffuse) light as well as a relatively complex view. Studies on what kind of components should be present in the viewed image have been done by many researchers, e.g. (Ulrich 1984; Ulrich et al. 1991; Tennessen and Cimprich 1995; Chang and Chen 2005; Aries et al. 2010). In their experimental studies, Tuaycharoen and Tregenza (2007) stated that view cannot be separated from the natural (day-) light itself.

Related to daylight and view, Hellinga and de Bruijn-Hordijk (2009) proposed certain quality levels, for themes that influence visual comfort, from A (the best) to D (the worst), which are also based on values found in the literature, e.g. (Kaplan and Kaplan 1989; Tregenza and Loe 1998). They proposed that for the view element, the best score will be achieved if the view contains the following: (1) green, sky, and distant objects, (2) maximum information about outside environment, such as weather, season, time of day, and (human) activities, and (3) complex and coherent image scene.

The use of a complex view on virtual windows in a laboratory environment to investigate the psychological effects has been explored by some researchers. In all of those experiments, the prototypes/displays were assumed to be the representation of what the subjects normally see through a real window. For example, IJsselsteijn et al. (2008), who focused on depth perception cues from screen projected images, used five image scenes, showing the presence of: (1) trees, ground, and three people standing, (2) trees and ground without people, (3)

creek, (4) desert, and (5) city skyline on a river at night. All scenes other than the last one display a daytime sky.

In their experiments on discomfort glare from projected images (Tuaycharoen and Tregenza 2005) used ten pairs of image scenes displaying either ‘natural’ (showing the presence of mountains, river, and/or trees) or ‘urban’ (showing the presence of buildings, i.e. houses, skyscrapers, castle, or school) views. A daytime sky (with or without clouds) is visible in every image scene. They concluded that a good view (also described as a view with high interest), which mainly consists of the natural scenes, tends to reduce discomfort glare perception.

Shin et al. (2012), who focused on subjective discomfort glare evaluation from a backlit, transparent printed image, used five pairs of image scenes displaying either ‘distant’ (i.e. the viewed objects are relatively faraway from the window) or ‘near’ (i.e. the viewed objects are relatively close to the window). The scene displayed a ‘mixed land’ (skyscrapers and trees), ‘man-made’ (skyscrapers), ‘mixed river’ (city skyline on a river), ‘natural land’ (trees and green ground), or ‘natural river’ (mountains or plants on a river). All pictures in the scenes were taken during daytime, but the sky was only (partly) visible on the ‘distant’ scenes, and not at all on the ‘near’ scenes. They concluded that the tolerance of discomfort glare sensation for the distant views including skyline was greater than the near views.

Considering the variation and clear distinction of the objects’ distance, the 10 image scenes of Shin et al. (2012) were incorporated to model the VNLS with complex views in this article. Some adaptations were made, including stretching, mirroring, and cropping the upper and lower part of the original image to get the same height of horizon (i.e. the border between the ground and the sky) in every image scene. The adapted image scenes are displayed in Figure 1.

While there are reported findings from various researchers on some aspects of VNLS prototypes and its impact to users, an objective study addressing the indoor lighting and visual comfort aspect is rare. The work described in this article focuses on the development and evaluation of a computational model of VNLS with complex views and directional light. It aims to demonstrate the role of computational modelling and building performance simulation in the research and development of such future solutions, by predicting the impact VNLS may have on the lighting performance in the test space.

In general, what this current study adds to the earlier study of (Mangkuto et al. 2014) is the introduction of 10 complex views in front of the light sources array; therefore applying the light and view on two separate layers. In particular, the objectives of this study are twofold. The first one is to understand the effect of changing input variables of the VNLS with complex views, which in this case are: the beam angle and total luminous flux of the ‘non-ground’ elements, and the image scenes, on the lighting performance of a reference office space. The second objective is to compare two techniques of modelling the view: using an ‘emissive’ approach, i.e. where the light sources are coloured and constructing the view itself, and using a ‘transmissive’ approach, i.e. where the light sources are all white and the view is made by pasting an image on a transparent surface in front of the sources. The transmissive approach was applied to generate the main result in this article, and the emissive approach was only calculated for the purpose of comparison.

The lighting performance is hereby described in terms of the ability to meet the space availability demand, the illuminance uniformity on the workplane, the illuminance contribution from the ground elements on the ceiling, and the ability to produce minimal glare at predefined observer’s positions in the space. Space availability is hereby defined as the percentage of workplane (at height of 0.75 m from the floor) meeting a certain minimum illuminance criteria.

## 2. Methods

### 2.1. Modelling

While all detailed characteristics of view from a window are considered very important for developing the requirement of VNLS, this study is focused on modelling the characteristics of direct light from a diffuse sky and reflected light from the exterior ground. In general, most of the existing virtual windows behave like a diffuse light source, reducing the possibility of seeing the impression of direct and reflected light components on the interior surface.

In the real sky, the luminous intensity highly depends on the sun's position and the sky turbidity, which are constantly changing over time. Natural light has a wide range of CCT which also varies over time in a day (Chain et al. 1999, Chain et al., 2001), from warm colours (red to yellowish white, during sunrise/sunset: 2700 ~ 3000 K) until cool colours (bluish white, during sunny day/around noon: 5000 ~ 6500 K; and blue, during overcast day or very blue sky condition: 6500 ~ 20000 K). The view through a real window is also dynamics. Certain quality levels for themes that influence visual comfort from a real window has been proposed by Hellinga and de Bruijn-Hordijk (2009), based on values found in the literature, e.g. (Kaplan and Kaplan 1989; Tregenza and Loe 1998).

Looking at those aspects, direction of further development of VNLS should be steered toward improving the light directionality and view dynamics. It is understood that a number of evaluation stages must be performed before the ideal solution can be obtained. In the early design stage, this article aims to demonstrate the role of computational modelling and simulation as a powerful tool to predict the system performance, with regards to the relevant physical phenomena. By using computational modelling and simulation, one is able to rapidly test multiple design concepts for better solutions, in an efficient way in terms of time and cost.

Therefore, we propose a model of VNLS in the form of an array of small directional light emitting areas that were tilted, as specified in the article of [Mangkuto et al. \(2014\)](#). To realise a complex view in the *Radiance* simulation tool, a two-dimensional image scene was imported and mapped on a very thin, vertically flat, transparent glass ( $\tau = 0.90$ ) material. This glass did not emit light itself, and was put in front of the light source array. Ten image scenes adapted from [Shin et al. \(2012\)](#) were used, as displayed in Figure 1.

In the model, the light sources of the ‘sky’ were arranged in 20 rows, in which the sources in the higher rows emitted more light than the ones in the lower rows. The bottom row acted as the ‘ground’ which is tilted upward to deliver the light to the ceiling. The rest of the sources acted as the ‘sky’ which was tilted downward to deliver the light to the workplane. The luminous intensity distribution of the sources is described in Figure 3, which corresponds to a certain value of average luminance of the display. All of the light sources were white in colour, which can be approximated by a correlated colour temperature (CCT) of 6500 K (daylight, overcast). The colour display was given by the mapped image. At the current stage, the light properties and view display were static, in a sense that the simulation was performed for one condition at a time.

The light emitting areas were modelled to fit two individual vertical openings, each with the size of  $0.80 \text{ m} \times 1.17 \text{ m}$  ( $W \times H$ ), corresponding to a window-to-wall ratio of 20%. Each light emitting area in each individual window had a size of  $0.05 \text{ m} \times 0.05 \text{ m}$  and had the role of lighting the ‘non-ground’ part of the image. At the lowest row, there were four light emitting areas ( $0.20 \text{ m} \times 0.20 \text{ m}$  each) to light the ‘ground’ part of the image. The entire array of light emitting areas was configured using the *xform* command in *Radiance*

To model the directionality of light entering through a window, the sources at the row directly above the ‘ground’ were at all times not tilted (i.e.  $0^\circ$ ), while the sources at the



second row above the ‘ground’ were tilted downward by 2.0°. The sources at the third row above the ‘ground’ were tilted downward by 4.0° and so forth. The ‘ground’ sources were always tilted with a 40° angle pointing upward.

Figure 2 displays the front and side views of the VNLS model.

The sources had a certain beam angle, i.e. the angle between the two directions opposed to each other over the beam axis for which the luminous intensity is half that of the maximum luminous intensity. Three values of beam angle (38°, 76°, 114°) for the ‘sky’ were introduced to represent a relatively narrow, medium, and wide spread. Based on the finding in the earlier article (Mangkuto et al. 2014), most of the VNLS with a beam angle of 76° yield a ratio of space availability of around 1.0, relative to the corresponding real window under the CIE overcast sky, which mean they perform the closest to real windows.

The luminous intensity distribution of each light source was written in an IES format file, based on the character of downlights with a certain beam angle. For the sources with a 114° beam angle, the distributions were set so that the combination of these sources, without the addition of the transparent glass, gives an average surface luminance ( $L$  [cd/m<sup>2</sup>]) of 1000 cd/m<sup>2</sup> (low luminance setting), 1800 cd/m<sup>2</sup> (medium), or 3200 cd/m<sup>2</sup> (high). These were the first three values used in the experiments of Shin et al. (2012). The intensity values for the ‘non-ground’ sources with 38° and 76° beam angles were adjusted accordingly, so that the total luminous flux coming from the ‘non-ground’ sources altogether remains the same. The total luminous flux from the source was then calculated based on the zonal cavity method described by Lindsey (1997).

For our case, the calculated total luminous fluxes of all ‘non-ground’ sources, without the addition of the transparent glass, are approximately 6200 lm, 11100 lm, and 19900 lm. Figure 3 displays the luminous intensity distributions of the ‘non-ground’ sources with total luminous flux of 11100 lm. The settings for each ‘ground’ source in this case were identical

with the case for VNLS with a simplified view, having a fixed beam angle of 76 degrees, and maximum intensity of 110 cd, 199 cd, and 354 cd for the three conditions respectively.

The variation in all input variables, including the image scene is summarised in Table 1. It should be noticed that the interval of tilt angle and the distance between windows are not considered as input variables that vary, since the finding in the case of VNLS with a simplified view suggests that both of them are less influential than the total luminous flux and beam angle (Mangkuto et al. 2014). In total, there are 90 possible combinations based on the input variables, taking the image scene variations into account.

## 2.2. Settings

The space discussed in this study was a reference office with dimensions of 5.4 m × 3.6 m × 2.7 m ( $L \times W \times H$ ). There was one window configuration, chosen from the studies of (Diepens et al. 2000) and (Lawrence Berkeley National Laboratory (LBL) 2010), as illustrated in Figure 4. There were frames of 5 cm wide at the perimeters of the windows.

Reflectance values of the room's interior were: ceiling: 85%, walls: 50%, floor: 20%, door: 50%, window and door frames: 50%; based on the IEA Task 27 reference office (van Dijk and Platzer 2003).

Three observer positions were defined at the eye height of 1.2 m above the floor, as illustrated in Figure 5. According to the finding in the case of VNLS with a simplified view (Mangkuto et al. 2014), position C, which directly faces the window plane, received the most severe discomfort glare. Therefore, the glare analysis was performed only for the observer at position C.

For all simulations, the parameters in *Radiance* were set as shown in Table 2.

## 2.3. Assessment

### 2.3.1. Performance indicators

The assessment for this study is based on the relevant performance indicators, which are:

- *Space availability (%A)*: the percentage of workplane area (at height of 0.75 m, with an equal size to the total floor area) with illuminance  $\geq 500$  lx (typical criteria for office work).

The %A is the percentage of the number of points with illuminance  $\geq 500$  lx ( $n(E \geq 500 \text{ lx})$ ), compared to the total number of points ( $N = 1944$ ).

$$\%A = \frac{n(E \geq 500 \text{ lx})}{N} \times 100\% \quad (1)$$

- *Uniformity ( $U_0$ )*: the ratio between the minimum illuminance ( $E_{min}$  [lx]) to the average ( $E_{av}$  [lx]), calculated based on the defined 1944 points.

$$U_0 = \frac{E_{min}}{E_{av}} \quad (2)$$

One of the advantages of applying VNLS in a space is the possibility to put multiple displays on any wall or ceiling surface, particularly in working spaces without access to the real façade due to hygienic or safety reasons, for instance in operating rooms in hospitals and control rooms in industrial plants. By doing so, a high uniformity within the workplane can be reasonably achieved, whereas the same thing is practically impossible in a sidelit room having only real windows on one façade. As a starting point, this study presents a case study with only one display on the short wall, which results can be further used for case studies with multiple displays and various placement configurations on the walls.

- *Ground contribution (%G)*: the percentage ratio of illuminance contribution from the ‘ground’ element sources ( $E_{ground}$  [lx]) to the total illuminance ( $E_{total}$  [lx]) received on a certain point on the ceiling, with the surface normal facing downward (z- axis). The  $E_{ground}$

was measured by removing the ‘sky’ elements in the model, leaving only the ‘ground’ ones. There are  $N = 10$  points on the ceiling, as illustrated in Figure 6. The average value is reported as  $\%G_{av}$ .

$$\%G = \frac{E_{ground}}{E_{total}} \times 100\% \quad (3)$$

$$\%G_{av} = \frac{\sum_{i=1}^N \%G_i}{N} \quad (4)$$

The VNLS model in this article basically follows the split-flux method for real windows under the CIE overcast sky (Tregenza 1989), in which the daylight component can be generally split into three parts, i.e. sky, externally reflected, and internally reflected components. The internally reflected component (IRC) enters through the window and reaches the point on the workplane after reflections from interior surfaces. It is known that this component partly comes from the exterior ground reflection. Therefore the VNLS model should also incorporate the ground reflection, which is evaluated using the metric of ‘ground contribution the ceiling’.

- *Probability of discomfort glare*: the normalised values of all potentially relevant glare metrics, i.e. Daylight Glare Probability (DGP), Daylight Glare Index (DGI), Unified Glare Rating (UGR), and CIE Glare Index (CGI), which were calculated with the *Evalglare* programme (Wienold and Christoffersen 2006), for the observer at position C in Figure 5. DGI was normalised into  $DGI_n$ , UGR into  $UGR_n$ , and CGI into  $CGI_n$ , following the normalisation procedures of Jakubiec and Reinhart (2012) to determine the ‘probability of discomfort glare’. The four normalised glare indices were then averaged, and the value was reported as the average probability of discomfort glare ( $PDG_{av}$ ). It should be noticed that the averaged value was calculated from the ‘normalised’ glare metrics, except for DGP,

since it is already normalised. The normalisation was applied to equalise the level of ‘uncomfortable’ perception in all of the metrics (Jakubiec and Reinhart 2012), in a way that all of the metrics are within a range of  $0 \sim 1$ .

$$PDG_{av} = (DGP + DGI_n + UGR_n + CGI_n) / 4 \quad (5)$$

The four glare metrics were taken into account since to the best of the authors’ knowledge, very little is known about which glare indices are most suited for the case of not-yet-existing VNLS models. Currently, the high accuracy of DGP compared to other glare metrics has been reported elsewhere, e.g. (Jakubiec and Reinhart 2012, Kleindienst and Andersen 2009), mainly due to the fact that DGP uses vertical illuminance on the observer’s eye as the main input. However, it is noticed that DGP also has some limitations. Next to the low availability of user acceptance study at lower luminance ranges (Wienold and Christoffersen 2006), it is also mentioned that DGP is less accurate for luminance contrast-based glare (Kleindienst and Andersen 2009), which typical example can be found in scenes with a generally low ambient illuminance, and with a high contrast point such as bright window glass with a dark frame. All of the earlier findings on DGP were also based on real daylight scenes only, as obviously implied in the metric’s name.

In the earlier article (Mangkuto et al. 2014), we have compared the  $PDG_{av}$  values for VNLS and real windows scene with the same average luminance, and found that the average and standard deviations in VNLS scenes are found to be very similar and never differing more than 0.01 from their real windows counterpart. In general, as shown in that article, the highest detected glare index among the four metrics (DGP,  $DGI_n$ ,  $UGR_n$ , and  $CGI_n$ ) was found to be the normalised CGI, while the lowest was found to be the DGP or the normalised DGI. As discussed by Jakubiec and Reinhart (2012), CGI was the most robust among the three metrics that have been developed earlier (DGI, UGR, CGI) as it

consistently predicted a higher likelihood of discomfort, thereby representing a worst-case comfort scenario. However, they also suggested that DGP responds predictably to most daylight situations, including those with many or large solid angle direct or specular luminance sources.

To this point, we argue that at the moment, a strong conclusion on the most appropriate glare metrics to be used for the VNLS models still cannot be drawn, as the models are specific and located in the border area between daylight and artificial lighting scenes. The use of  $PDG_{av}$  as a metric is proposed here to compensate the possible difference in glare perception that may be expected in VNLS scenes.

### ***2.3.2. Sensitivity analysis of transmissive approach***

Sensitivity analysis using multiple linear regressions was performed to evaluate the influencing effect of the current input variables on the defined performance indicators. This regression model assumes a linear relationship between the output variable  $y_i$  and the  $p$ -vector of input variables  $x_i$ . The mathematical model reads as follows:

$$y_i = \beta_1 x_{i1} + \beta_2 x_{i2} + \varepsilon_i \quad , \quad i = 1, 2, \dots, 9 \quad (6)$$

where  $\beta_i$  is a  $p$ -dimensional regression coefficient. In this case:  $p = 2$ ,  $n = 3 \times 3 = 9$ ,  $x_1$  is the beam angle (BA, in degrees), and  $x_2$  is the total luminous flux ( $\Phi$ , in lumens); while  $y$  is evaluated individually for  $\%A$ ,  $U_0$ ,  $\%G_{av}$ , and  $PDG_{av}$ . The calculation was performed individually for the 10 image scenes, i.e. no mix between different image scenes.

The values were standardised, and then are put in the regression model expressed in the matrix form as follows:

$$\begin{bmatrix} y_1' \\ \dots \\ y_n' \end{bmatrix} = \begin{bmatrix} x_{11}' & x_{12}' \\ \dots & \dots \\ x_{n1}' & x_{n2}' \end{bmatrix} \begin{bmatrix} \beta_1' \\ \beta_2' \end{bmatrix} + \begin{bmatrix} \varepsilon_1' \\ \dots \\ \varepsilon_n' \end{bmatrix}, \quad n = 9 \quad (7)$$

The equations were then solved using a MATLAB toolbox to determine  $\beta_1'$  and  $\beta_2'$ , which are the standard regression coefficients that determine the sensitivity of the output, i.e. BA and  $\Phi$  respectively, as function of the input. The values range from 1 (strong, positive influence) to  $-1$  (strong, negative influence).

### 2.3.3. Comparison of transmissive and emissive approaches

As mentioned in the Introduction part, the second objective of this study is to compare the approach of modelling a view on VNLS, by observing the effect on the lighting performance. In the earlier article (Mangkuto et al. 2014), the ‘emissive’ approach was applied to model the VNLS with a simplified view. In that case, the light sources were either blue or green-coloured in order to construct the view of the blue sky and green ground. In this article, we introduce the ‘transmissive’ approach, where the light sources are all white and do not build the view themselves. The view is realised by pasting a two-dimensional image on a transparent, glass surface in front of the sources. It is then intended to know the impact of using these two approaches on the lighting performance of the given space.

To make the comparison, two characteristically different image scenes were introduced, which are: (1) a blue sky and green ground (referred as BG), and (2) a green ‘sky’ (entirely obstructed) and blue ‘ground’ (referred as GB), as in a simplified view of green trees on a river, seen from a relatively near distance. The image scenes are illustrated in Figure 7. In the GB scene, the general composition of blue and green colours is inverted, the sky is entirely covered, but the ‘ground’ may appear brighter instead.

The image scenes were drawn using the Colour Picker from JALOXA website (Jacobs 2012a), where colour properties are given in red, green, and blue values between 0 ~ 1 as used in *Radiance*. If these values are seen as the spectral reflectance of a given material, then the weighted average reflectance ( $\rho$ ), which takes the human eye's spectral sensitivity into account, can be obtained using the formula described by (Jacobs 2012b):

$$\rho = 0.265 \rho_R + 0.670 \rho_G + 0.065 \rho_B \quad (8)$$

where  $\rho_R, \rho_G, \rho_B$  are respectively the spectral reflectance in red, green, and blue. By analogy, a similar expression can be applied for relating the weighted average transmittance and spectral transmittance of a given material, which is the case for the transmissive approach. The equation then reads as follows:

$$\tau = 0.265 \tau_R + 0.670 \tau_G + 0.065 \tau_B \quad (9)$$

The red, green, and blue properties of each transmissive element of both image scenes in Figure 7 are described in Table 3.

As shown in Table 3, the shade of green in the GB scene is exactly equal to that in the BG scene, as intended and displayed in Figure 7. To display a darker colour using the emissive approach, one needs to reduce the luminous intensity of the source, hence also reduce the total luminous flux. However, in this comparison, we opt to have the same total luminous flux of the light sources in both approaches, which corresponds to the same total input power of the sources.

In the emissive approach, the light emitting areas were created from standard IES files describing the luminous intensities at all relevant angles, then converted into standard *Radiance* object files using the programme *ies2rad*. By default, the light emitting areas are defined as 'glow' materials with colour properties of (1, 1, 1), i.e. white. To change the



colour, one may use the colour properties as suggested by JALOX, but the values should be normalised with their weighted average value, before inserting in *Radiance*. This is necessary to ensure the final weighted average value stays equal to 1, thus maintaining correct values for the resulting luminances (Jacobs 2012b). For example, to display a light-blue colour of (0.5, 0.8, 1), one has to calculate the weighted average transmittance value using Equation 9, which gives 0.734. The normalised values are then (0.5/0.734, 0.8/0.734, 1/0.734), or (0.682, 1.091, 1.363). These values should be filled in the *Radiance* object file of the light source, replacing the default values of (1, 1, 1).

The input variables were beam angle of 38°, 76°, and 114°, interval of tilt angle of 2.0°, and total luminous flux of the ‘non-ground’ elements of 11100 and 19900 lm. In the emissive approach, the models were built by assigning the relevant colours to the light sources; while in the transmissive approach, the relevant image in Figure 7 was pasted on the glass surface in front of the white light sources. Note that for the latter approach, the total luminous flux of the ‘non-ground’ elements belongs to the light sources only, without considering the transparent glass surface.

For all variations, simulations were performed to evaluate the four performance indicators mentioned in Section 2.3.2.

### 3. Results and Discussion

Figure 8 displays a selection of the results of the space availability (% $A$ ), uniformity ( $U_0$ ), average ground contribution (% $G_{av}$ ), and average probability of discomfort glare (PD $G_{av}$ ) for all window variations/configurations with total luminous flux of 11100 lm in the transmissive VNLS case.

### 3.1. Transmissive approach

The standard regression coefficients ( $\beta$ ) of all input variables, i.e. beam angle (BA) and total luminous flux ( $\Phi$ ), are shown in Figure 9. They are evaluated for the four performance indicators, i.e.  $\%A$ ,  $U_0$ ,  $\%G_{av}$ , and  $PDG_{av}$ , under the 10 image scenes.

As illustrated in Figure 9, total luminous flux ( $\Phi$ ) is the most influential input variable to the space availability, while beam angle (BA) is the most influential input variable to the other output variables, independent of the image scene. It is however noticed that under the scenes of ‘Near Natural Land’ and ‘Near Natural River’, the standard regression coefficients ( $\beta$ ) for total luminous flux related to space availability are respectively 0.56 and 0.59, while the value under other scenes is always larger than 0.80, which is discussed later on. Figure 10 displays the graphs showing the relationship between mean values of the output and the most influential input variable(s) with a 95% confidence level, under the 10 image scenes.

#### 3.1.1. Space availability

The space availability is highly, positively influenced ( $\beta = 0.56 \sim 0.96$ , depends on the image scene) by the total luminous flux of the ‘non-ground’ elements. The largest values are achieved under the ‘Near Mixed River’ and ‘Distant Natural River’ scene, where a total luminous flux of 19900 lm will create a space availability of around 27% and 24%, respectively. The mean space availability values increase with a factor of 4.0 (under NMR scene) and 5.0 (under DNR scene) when increased from 6200 lm to 11100 lm, then 2.2 (NMR) and 2.4 (DNR) when increased from 11000 lm to 19900 lm. Both image scenes provide either a large white-coloured area (i.e. the skyscraper buildings’ façade in NMR) or a large, light bluish-coloured area (i.e. the sky in DNR). Hence, more light is transmitted through the image plan, generating a larger area with illuminance exceeding 500 lx.

On the other side of the scale, the ‘Near Natural Land’ and ‘Near Natural River’ scenes generate the smallest space availability, which is only 1% and 3% when the total luminous flux is 19900 lm, and zero when the total luminous flux is lower. Both scenes have the sky entirely covered with dark-coloured objects, which in this case are green trees or red plants on a hill. Those elements reduce most of the light transmission, resulting in a low value of space availability. Under these two scenes, increasing total luminous flux does not necessarily increase the space availability, which in turn makes the standard regression coefficient not as large as under the other eight scenes.

### ***3.1.2. Uniformity***

The uniformity is highly, positively influenced ( $\beta' = 0.75 \sim 1.00$ ) by the beam angle of the ‘non-ground’ elements. Under a given scene and with a given beam angle, the uniformity practically stays the same when the total luminous flux is changed. The minimum and average illuminance values on the workplane are directly proportional to the total light output of the source, hence the constant value of uniformity. On average, the ‘Near Natural Land’ and ‘Near Natural River’ scenes generate the largest uniformity, which are 0.44 and 0.48 for beam angle of  $114^\circ$ . While both scenes have the sky entirely covered with relatively uniform, dim objects (i.e. green trees or red plants), the resulting minimum and average illuminance values on the workplane are also relatively close to each other.

Under the other eight scenes, the uniformity values range from 0.12 to 0.19 for beam angle of  $38^\circ$ , 0.22 to 0.28 ( $76^\circ$ ), and 0.32 to 0.38 ( $114^\circ$ ). The relationship between the beam angle and uniformity is almost perfectly linear under all image scenes.

### **3.1.3. Ground contribution on the ceiling**

The average ground contribution on the ceiling is highly, negatively influenced ( $\beta' = -0.91 \sim -0.97$ ) by the beam angle, quite independent of the image scene. As found for the uniformity, under a given scene and with a given beam angle, the average ground contribution on the ceiling stays constant when the total luminous flux is changed. A similar trend is also observed in terms of the image scenes creating the largest %G values. The ‘Near Natural Land’ and ‘Near Natural River’ scenes generate the largest average ground contribution on the ceiling, which are respectively 73% and 78% for beam angle of 38°, 65% and 70% (76°), and 64% and 67% (114°). In both scenes, the view is almost entirely filled with dim objects (i.e. green trees or red plants), but the ‘ground’ part (i.e. light green grass or blue river) actually appears brighter than the ‘non-ground’ part. This results in a larger contribution of illuminance values on the ceiling, compared to the contribution of the ‘non-ground’ part.

Meanwhile, in the other scenes, the ‘ground’ part is generally darker than the ‘non-ground’ part, creating a lower value of average ground contribution. The scenes of ‘Near Mixed Land’ and ‘Distant Natural River’ generate the smallest average ground contribution on the ceiling, which are respectively 30% and 34% for beam angle of 38°, 21% and 22% (76°), and 17% and 19% (114°).

### **3.1.4. Probability of discomfort glare**

The average probability of discomfort glare is highly, negatively influenced ( $\beta' = -0.78 \sim -0.89$ ) by the beam angle. Figure 9d shows that at a given beam angle, the values under various image scenes are nearly the same, except again under the ‘Near Natural Land’ and ‘Near Natural River’ scenes, which give lower values. For example, the two scenes give

average probability of discomfort glare of 0.33 and 0.32 (beam angle of 38°), while the figures are between 0.35 and 0.40 under the other scenes with the same beam angle. As explained earlier, both scenes have the sky entirely covered with relatively dim objects (i.e. green trees or red plants), thus effectively reducing the light transmitted, which in turns also consequently reduce the space availability and glare perception. The relationship between the beam angle and probability of discomfort glare is almost perfectly linear under all image scenes.

While the results of the sensitivity analysis seem to be obvious, the quantitative influence of each input parameter on each output variables under various image scenes can be obtained only by conducting simulation. An interesting example is the probability of discomfort glare; theoretically, as well as empirically, one can assume that the more light output coming from the display, the more discomfort glare it will create. The reverse can be assumed for beam angle; the larger the beam angle, the less discomfort glare. These are indeed also found in the simulation. However, it turns out from the sensitivity analysis that the beam angle is actually the most influential factor on discomfort glare, and not the total luminous flux. One potential reason is that the probability of discomfort glare is mostly dominated by the amount of contrast, and increasing beam angle will result in reducing contrast. Based on the performed simulation, one can decide better on which input variables to focus on, with regard to a certain output variables; rather than merely guessing based on visual observation.

Another rationale of using such approach is the amount of time that can be saved in evaluating various input alternatives, which may include more complex situations where interactions can become hard to visually observe and theoretically forecast. As mentioned earlier, the process of developing such a future solution is lengthy. The use of modelling and

simulation is important in influencing the design direction, particularly in the early stage; therefore it deserves to be discussed on its own.

Figure 11 displays the rendered impression (visualised with mimicked human visual response), observed from position C, of three selected image scenes, i.e. 'Near Mixed River', 'Near Natural Land', and 'Near Natural River', with beam angle of 38°, 76°, 114°, and total luminous flux of 19900 lm, using the transmissive approach. The image rendering process was run with simulation parameters as listed in Table 2, but with ambient divisions of 10000. Some random splotches can be observed on the side walls in Figure 11, particularly in configurations with the beam angle of 76°. In configurations with the beam angle of 38°, most of the delivered light is focused around the lateral axis of the room; therefore the side walls are relatively dark. In configurations with the beam angle of 114°, the delivered light is almost evenly spread on the interior surface; therefore the side walls appear much brighter. In configurations with the beam angle of 76°, the situations are in between; therefore the rendered images contain the most random splotches. According to [Jacobs \(2012c\)](#) and [Compagnon \(1997\)](#), as the light source gets smaller, the required number of ambient sample rays exponentially increases. Nonetheless, for a particularly large amount of very small sources such as in this case, the stochastic sampling can become too computationally intensive; therefore we do not proceed with higher numbers of ambient divisions.

### **3.2. Comparison of transmissive and emissive approaches**

Table 4 summarises the space availability, uniformity, average ground contribution, and average probability of discomfort glare of the 'blue sky and green ground' (BG) and 'green obstructed sky and blue ground' (GB) image scenes as shown in Figure 8; and the modelling

approaches, i.e. transmissive and emissive; all with total luminous flux of 11100 and 19900 lm.

Table 4 shows that with the emissive approach, given the same beam angle and total luminous flux, the performance indicators do not change when a different image scene is displayed. To display various colours of a ‘glow’ material in *Radiance*, one can edit the red, green, and blue radiance components of the sources, but they have to be normalised using the procedure given by (Jacobs 2012b), so that two light sources with the same light output will produce the same illuminance values on the same point, even though the sources have different colours.

The consequence of using this technique of producing colours from light is that darker colours can only be realised by reducing the luminous intensity. In practice, one may not get the intended dark colours; for example a completely black colour will be difficult to display, instead it may just become a dark grey. Nevertheless, the comparison between the 10 image scenes of Shin et al. (2012) shows that the presence of light-coloured, and not the dark-coloured, objects in the view is what important in improving the space availability.

Using the transmissive approach, the light output is reduced by the transparent glass on which the image scene is pasted. It is clearly shown that the GB scene reduces a significant amount of light, compared to the BG scene. As a result, the space availability under the GB scene is much smaller than that under the BG scene. In turn, the ground contribution under the GB scene is relatively large, due to the fact that the ‘ground’ part appears brighter than the rest of the display. The probability of discomfort glare under the GB scene is smaller than that under the BG scene, obviously due to the smaller amount of light transmitted from the window display.

To understand the difference between the two approaches, Table 4 can be further simplified by showing the ratio of each performance indicator obtained using the transmissive

approach, compared to the one obtained using the emissive approach, for a given beam angle and total luminous flux. These ratio values are displayed in Table 5.

It can be seen from Table 5, that under the BG scene, the space availability using the transmissive approach is around 30% ~ 50% of the corresponding values using the emissive approach. Under the GB scene, the space availability using the transmissive approach is very near or equal to zero. It should be noticed however that the space availability is calculated based on 500 lx as minimum criterion; hence a value of zero does not necessarily imply that the entire workplane has zero illuminance, but the maximum illuminance is certainly smaller than 500 lx. Moreover, even though the glass transmittance for all cases is fixed at  $\tau = 0.90$ , the actual light transmitted by the display is apparently much less than this proportion, due to an additional reduction which largely depends on the view elements of the image scene.

The uniformity and ground contribution under the GB scene is slightly larger when using the transmissive approach, compared to the emissive one; while the opposite is true under the BG scene. Under both scenes, the average probability of discomfort glare using the transmissive approach is around 70% ~ 90% of the values obtained using the emissive approach.

To give a clearer illustration, Figure 12 displays some rendered impression of the scenes (visualised with mimicked human visual response) with total luminous flux of 19900 lm and  $BA = 114^\circ$ , under both the BG and GB image scenes, using the emissive and transmissive approach. In the scenes using the emissive approach, the side walls show a strong impression of the colour of the ‘non-ground’ elements, i.e. blue under the BG scene and green under the GB scene. The floor area near the window appears less bright and less bluish/greenish in the scenes using the transmissive approach, due to the light reduction by the display. While the emissive approach generally creates larger space availability, it also generates more contrast



between the display and its immediate surrounding, which leads to a larger probability of discomfort glare.

#### 4. Conclusions and Outlook

We have proposed a computational model of VNLS configurations with complex views, where the light is provided by arrays of white-coloured directional light emitting sources with specific tilt angles, and the view is provided by mapping a two-dimensional image on a transparent glass in front of the light sources. Comparisons are shown between 10 image scenes adapted from [Shin et al. \(2012\)](#), to evaluate the lighting performance indicators, i.e. space availability, uniformity, average ground contribution, and average probability of discomfort glare, using a transmissive approach.

In turn, it is concluded that:

- Under every image scene, the total luminous flux of the ‘non-ground’ element is largely influential to the space availability (standard regression coefficient  $\beta' = 0.56 \sim 0.96$ ).
- Under every image scene, the beam angle of the ‘non-ground’ element is largely influential to the uniformity ( $\beta' = 0.75 \sim 1.00$ ), average ground contribution on the ceiling ( $\beta' = -0.91 \sim -0.97$ ), and average probability of discomfort glare ( $\beta' = -0.78 \sim -0.89$ ).
- The quantitative influence of each input parameter on each output variables under various image scenes can be obtained by conducting simulation. The average probability of discomfort glare is an example; it turns out from the sensitivity analysis, that the metric is mostly influenced by the beam angle and not the total luminous flux. It is mostly dominated by the amount of contrast, and increasing beam angle will result in reducing contrast. Based on the performed simulation, one can decide better on which input variables to focus on, with regard to a certain output variables.

- The largest space availability is achieved under the scenes displaying a large white-coloured or light bluish-coloured area, as found in the examples of ‘Near Mixed River’ and ‘Distant Natural River’ scenes; while the smallest is achieved under the scenes displaying dark-coloured objects dominating the entire view, as found in the examples of ‘Near Natural Land’ and ‘Near Natural River’ scenes. In turn, the ‘Near Natural Land’ and ‘Near Natural River’ scenes generate the largest uniformity and ground contribution on the ceiling, as well as the smallest probability of discomfort glare.

The findings lead to a suggestion of preferred elements in the image scene, which are large, light-coloured ‘non-ground’ (such as a blue sky) and light-coloured ‘ground’ (such as light-green grass or light-blue river), to ensure large space availability, uniformity, and ground contribution on the ceiling. An adjustment on the luminous flux of the light source is however necessary to reduce the probability of discomfort glare.

Comparison of the emissive and transmissive approach using a simplified view scene (BG or GB), shows that the transmissive approach generally results in smaller values of space availability, relative to the emissive one. The actual light transmitted largely depends on the colour of the view elements of the image scene. In turn, the average probability of discomfort glare using the transmissive approach is smaller than that using the emissive approach.

These findings can give some ideas on what kind of performance ranges future VNLS would bring. The use of an emissive approach may introduce more light inside the space, but the view complexity is limited by the number of pixels or individual elements. If this limitation can be addressed in the future, then this approach will be the reasonable choice. On the other hand, the transmissive approach offers more flexibility to apply complex views on the display, but also requires more light, and thus consumes more energy to satisfy the lighting criteria.

In the end, it is noticed that subjective user evaluations are required to understand how people will appraise VNLS in reality, which is not addressed in this article. Despite the limitation, the presented results show clear examples of how building performance simulation contributes in the research and development of future solutions, by demonstrating the range of possibilities offered by the numerical model of VNLS, and how they compare to each other.

## References

- Aries MBC, Veitch JA, Newsham G (2010). Windows, view, and office characteristics predict physical and psychological discomfort. *Journal of Environmental Psychology*, 30: 533-541.
- Boyce PR, Hunter C, Howlett O (2003). The Benefits of Daylight Through Windows. Capturing the Daylight Dividend Program.
- CEN (2002). EN 12464-1: Light and Lighting - Lighting of work places, Part 1: Indoor work places. Brussels: Comité Européen de Normalisation.
- Chain C, Dumortier D, Fontoynt M (1999). A comprehensive model of luminance, colour temperature and spectral distribution of skylight – comparison with experimental data. *Solar Energy*, 65: 285-295.
- Chain C, Dumortier D, Fontoynt M (2001). Consideration of daylight's colour. *Energy and Buildings*, 33: 193-198.
- Chang C-Y, Chen P-K (2005). Human response to window views and indoor plants in the workplace. *HortScience*, 40: 1354-1359.
- Compagnon R (1997). Radiance Course on Daylighting. Available via <http://radsite.lbl.gov/radiance/refer/rc97tut.pdf>. Accessed 18 Feb 2014.
- Diepens JFL, Bakker F, Zonneveldt L (2000). Daylight Design Variations Book. TNO-TUE Centre for Building Research. Available via <http://sts.bwk.tue.nl/daylight/varbook/index.htm>. Accessed 21 Nov 2013.
- Hellinga HY, de Bruijn-Hordijk GJ (2009). A new method for the analysis of daylight access and view out. In: Proceedings of Lux Europa 2009 - the 11<sup>th</sup> European Lighting Conference. Istanbul: Turkish National Committee on Illumination.
- Heschong L (2003). Window and Offices: A Study of Office Worker Performance and the Indoor Environment. California, USA: Heschong Mahone Group.
- Heschong L, Wright RL, Okura S (2002). Daylighting impacts on human performance in school. *Journal of the Illuminating Engineering Society*, 31: 101-114.
- IJsselsteijn WA, Oosting W, Vogels I, de Kort YAW, van Loenen EJ (2008). A room with a cue: The efficacy of movement parallax, occlusion, and blur in creating a virtual window. *PRESENCE*, 17: 269-282.
- Jacobs A (2012a). Colour Picker for *Radiance*. Available via [http://www.jaloxa.eu/resources/radiance/colour\\_picker.shtml](http://www.jaloxa.eu/resources/radiance/colour_picker.shtml). Accessed 21 Nov 2013.
- Jacobs A (2012b). RADIANCE Cookbook. Available via [http://www.jaloxa.eu/resources/radiance/documentation/docs/radiance\\_cookbook.pdf](http://www.jaloxa.eu/resources/radiance/documentation/docs/radiance_cookbook.pdf). Accessed 21 Nov 2013.
- Jacobs A (2012c). RADIANCE Tutorial. Available via [http://www.jaloxa.eu/resources/radiance/documentation/docs/radiance\\_tutorial.pdf](http://www.jaloxa.eu/resources/radiance/documentation/docs/radiance_tutorial.pdf). Accessed 21 Nov 2013.
- Jakubiec JA, Reinhart CF (2012). The 'adaptive zone' – A concept for assessing discomfort glare throughout daylight spaces. *Lighting Research and Technology*, 44: 149-170.

- Kaplan R, Kaplan S (1989). *The Experience of Nature: A Psychological Perspective*. Cambridge: Cambridge University Press.
- Lawrence Berkeley National Laboratory (LBL). (2010). Virtual Lighting Simulator. Available via <http://gaia.lbl.gov/vls/>. Accessed 21 Nov 2013.
- Lindsey JL (1997). *Applied Illumination Engineering*. Lilburn: The Fairmont Press, Inc.
- Mangkuto RA, Aries MBC, van Loenen EJ, Hensen JLM (2014). Simulation of virtual natural lighting solutions with a simplified view. *Lighting Research and Technology*, 46: 198-218.
- Shin JY, Yun GY, Kim JT (2012). View types and luminance effects on discomfort glare assessment from windows. *Energy and Buildings*, 46: 139-145.
- Tennessen CM, Cimprich B (1995). Views to nature: Effects on attention. *Journal of Environmental Psychology*, 15: 77-85.
- Tregenza PR (1989). Modification of the split-flux formulae for mean daylight factor and internal reflected component with large external obstructions. *Lighting Research and Technology*, 21: 125-128.
- Tregenza PR, Loe D (1998). *The Design of Lighting*. London: E & FN Spon.
- Tuaycharoen N, Tregenza PR (2005). Discomfort glare from interesting images. *Lighting Research and Technology*, 37: 329-341.
- Tuaycharoen N, Tregenza PR (2007). View and discomfort glare from windows. *Lighting Research and Technology*, 39: 185-200.
- Ulrich RS (1984). View through a window may influence recovery from surgery. *Science*, 224: 420-421.
- Ulrich RS, Simons RF, Losito BD, Fiorito E, Miles MA, Zelson M (1991). Stress recovery during exposure to natural and urban environments. *Journal of Environmental Psychology*, 11: 201-230.
- van Dijk D, Platzer WJ (2003). Reference office for thermal, solar and lighting calculations. Report no. swift-wp3-tno-dvd-030416.
- Ward G, Shakespeare RA (1998). *Rendering with Radiance: The Art and Science of Lighting Visualization*. San Francisco: Morgan Kaufman Publishers.
- Wienold J, Christoffersen J (2006). Evaluation methods and development of a new glare prediction model for daylight environments with the use of CCD cameras. *Energy and Buildings*, 38: 743-757.

**Table 1** Input variables and their values variation

Variable	Symbol	Unit	Values
Beam angle	BA	deg	38, 76, 114
Total luminous flux	$\Phi$	lm	6200, 11100, 19900
Image scene	-	-	DML, NML, DMR, NMR, DMM, NMM, DNL,>NNL, DNR, NNR

**Table 2** *Radiance* simulation parameters

Parameter	Description	Value
-ab	Ambient bounces	4
-aa	Ambient accuracy	0.08
-ar	Ambient resolution	128
-ad	Ambient divisions	1024
-as	Ambient super-samples	256
-ds	Direct sub-sampling	0.2

**Table 3** Red, green, and blue properties of each transmissive element of the BG and GB image scenes

Scene	Element	Red	Green	Blue	Average
BG	'Sky'	0.500	0.800	1.000	0.734
BG	'Ground'	0.300	0.500	0.200	0.428
GB	'Sky'	0.300	0.500	0.200	0.428
GB	'Ground'	0.500	0.800	1.000	0.734

**Table 4** Summary of  $\%A$ ,  $U_0$ ,  $\%G_{av}$ , and  $PDG_{av}$  of each VNLS configuration with the BG and GB image scenes, using emissive and transmissive approaches

<b>Approach</b>	<b>Scene</b>	<b>BA</b> [°]	<b><math>\Phi</math></b> [lm]	<b><math>\%A</math></b> [%]	<b><math>U_0</math></b> [-]	<b><math>\%G_{av}</math></b> [%]	<b><math>PDG_{av}</math></b> [-]
Transmissive	BG	38	11100	17	0.18	49	0.37
Emissive	BG	38	11100	32	0.21	61	0.43
Transmissive	BG	76	11100	13	0.27	38	0.28
Emissive	BG	76	11100	31	0.28	50	0.38
Transmissive	BG	114	11100	9	0.37	35	0.25
Emissive	BG	114	11100	28	0.37	49	0.35
Transmissive	GB	38	11100	0	0.26	64	0.33
Emissive	GB	38	11100	32	0.21	61	0.43
Transmissive	GB	76	11100	0	0.35	55	0.26
Emissive	GB	76	11100	31	0.28	50	0.38
Transmissive	GB	114	11100	0	0.42	54	0.23
Emissive	GB	114	11100	28	0.37	49	0.35
Transmissive	BG	38	19900	32	0.18	49	0.41
Emissive	BG	38	19900	72	0.21	60	0.46
Transmissive	BG	76	19900	31	0.26	38	0.30
Emissive	BG	76	19900	70	0.28	50	0.41
Transmissive	BG	114	19900	28	0.37	35	0.27
Emissive	BG	114	19900	59	0.37	49	0.37
Transmissive	GB	38	19900	7	0.25	64	0.36
Emissive	GB	38	19900	72	0.21	60	0.46
Transmissive	GB	76	19900	4	0.35	55	0.28
Emissive	GB	76	19900	70	0.28	50	0.41
Transmissive	GB	114	19900	2	0.44	54	0.25
Emissive	GB	114	19900	59	0.37	49	0.37

**Table 5** Ratio of  $\%A$ ,  $U_0$ ,  $\%G_{av}$ , and  $PDG_{av}$  of each VNLS configuration with the BG and GB image scenes using the transmissive approach (subscript t), compared to those using the emissive approach (subscript e)

Scene	BA [°]	$\Phi$ [lm]	$\frac{\%A_t}{\%A_e}$	$\frac{U_{0_t}}{U_{0_e}}$	$\frac{\%G_{av_t}}{\%G_{av_e}}$	$\frac{PDG_{av_t}}{PDG_{av_e}}$
BG	38	11100	0.5	0.9	0.8	0.9
BG	76	11100	0.4	1.0	0.8	0.7
BG	114	11100	0.3	1.0	0.7	0.7
GB	38	11100	0.0	1.2	1.1	0.8
GB	76	11100	0.0	1.2	1.1	0.7
GB	114	11100	0.0	1.1	1.1	0.7
BG	38	19900	0.4	0.9	0.8	0.9
BG	76	19900	0.4	0.9	0.8	0.7
BG	114	19900	0.5	1.0	0.7	0.7
GB	38	19900	0.1	1.2	1.1	0.8
GB	76	19900	0.1	1.2	1.1	0.7
GB	114	19900	0.0	1.2	1.1	0.7



## List of Figures

**Fig. 1** Image scenes adapted from [Shin et al. \(2012\)](#): (a) ‘Distant Mixed Land’ (DML), (b) ‘Near Mixed Land’ (NML), (c) ‘Distant Man-made’ (DMM), (d) ‘Near Man-made’ (NMM), (e) ‘Distant Mixed River’ (DMR), (f) ‘Near Mixed River’ (NMR), (g) ‘Distant Natural Land’ (DNL), (h) ‘Near Natural Land’ (NNL), (i) ‘Distant Natural River’ (DNR), (j) ‘Near Natural River’ (NNR) (available online in colour)

**Fig. 2** Front and side views of the VNLS

**Fig. 3** Polar diagram of luminous intensity (in candela) of the sources that light the ‘non-ground’ area of the mapped image scene, with total luminous flux of 11100 lm and beam angle of (a) 38°, (b) 76°, and (c) 114°

**Fig. 4** Elevation view of the VNLS window configuration on the wall

**Fig. 5** (a) Plan view and (b) section view of the simulated space

**Fig. 6** (a) Plan view and (b) section view of calculation points for ground contribution

**Fig. 7** Image scenes of (a) ‘blue sky and green ground’ (BG) and (b) ‘green obstructed sky and blue ground’ (GB)

**Fig. 8** Summary of (a) space availability, (b) uniformity, (c) average ground contribution, and (d) probability of discomfort glare for all variations under the 10 image scenes of VNLS with  $\Phi = 11100$  lm

**Fig. 9** Standard regression coefficient of all input variables (i.e. BA and  $\Phi$ ), evaluated for the four performance indicators, i.e. (a) %A, (b)  $U_0$ , (c) % $G_{av}$ , and (d) PDG $_{av}$  under the 10 image scenes

**Fig. 10** Graphs showing the relationship between arithmetic mean of the output (i.e. %A,  $U_0$ , % $G_{av}$ , and PDG $_{av}$ ) and the most influential input variable(s), with a 95% confidence level

**Fig. 11** Impression of three image scenes, all with  $\Phi = 19900$  lm: (a) NMR, BA = 38°; (b) NMR, BA = 76°; (c) NMR, BA = 114°; (d) NNL, BA = 38°; (e) NNL, BA = 76°; (f) NNL, BA = 114°; (g) NNR, BA = 38° (h) NNR, BA = 76°; (i) NNR, BA = 114°

**Fig. 12** Impression of the BG and GB image scenes with emissive and transmissive approach, all with  $\Phi = 19900$  lm and BA = 114°

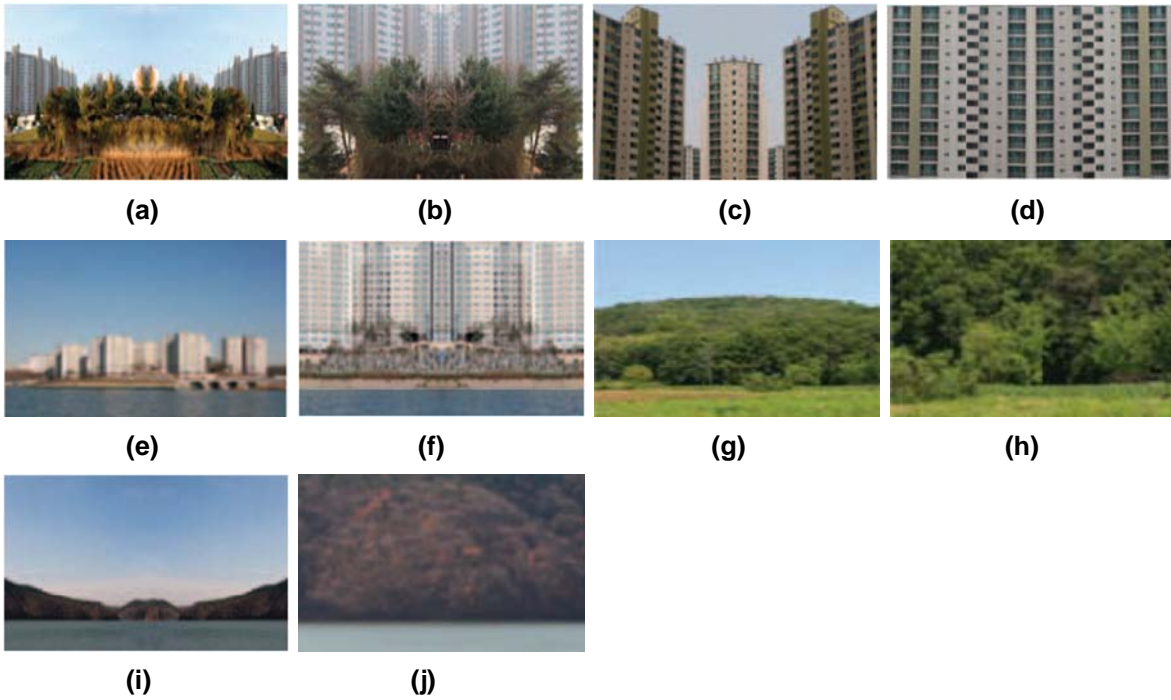


**Fig. 1** Image scenes adapted from [Shin et al. \(2012\)](#): (a) ‘Distant Mixed Land’ (DML), (b) ‘Near Mixed Land’ (NML), (c) ‘Distant Man-made’ (DMM), (d) ‘Near Man-made’ (NMM), (e) ‘Distant Mixed River’ (DMR), (f) ‘Near Mixed River’ (NMR), (g) ‘Distant Natural Land’ (DNL), (h) ‘Near Natural Land’ (NNL), (i) ‘Distant Natural River’ (DNR), (j) ‘Near Natural River’ (NNR) (available online in colour)

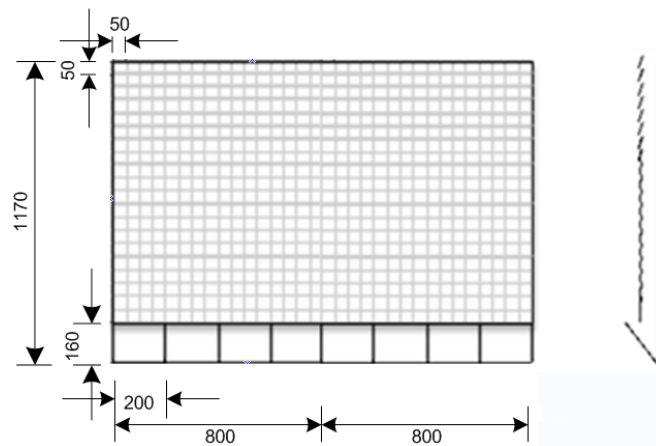


**Fig. 2** Front and side views of the VNLS

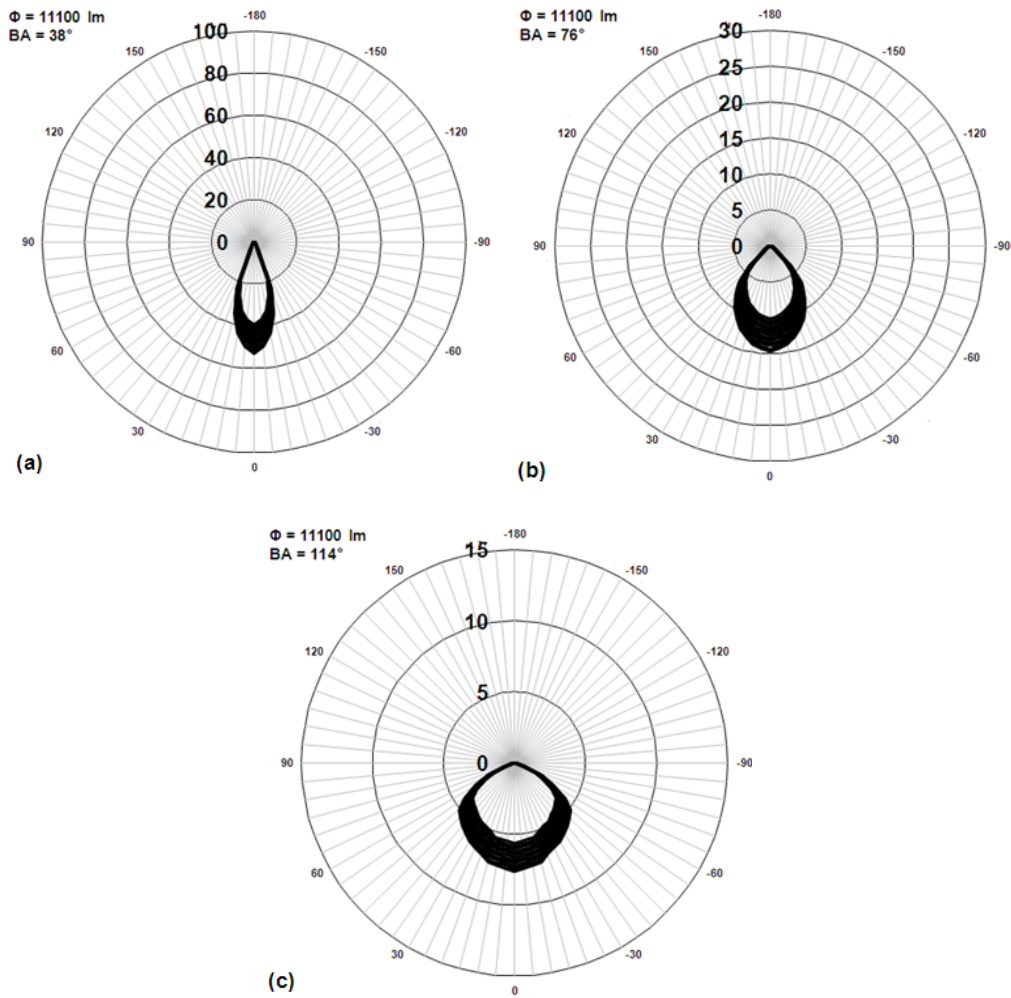


**Fig. 3** Polar diagram of luminous intensity (in candela) of the sources that light the ‘non-ground’ area of the mapped image scene, with total luminous flux of 11100 lm and beam angle of (a)  $38^\circ$ , (b)  $76^\circ$ , and (c)  $114^\circ$

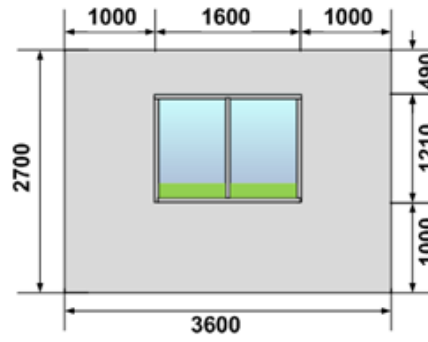


**Fig. 4** Elevation view of the VNLS window configuration on the wall

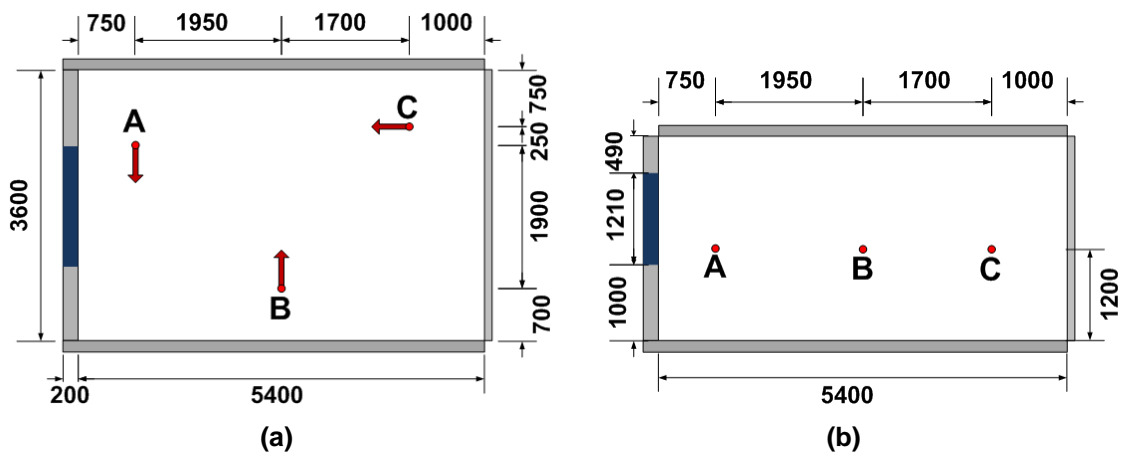


**Fig. 5** (a) Plan view and (b) section view of the simulated space

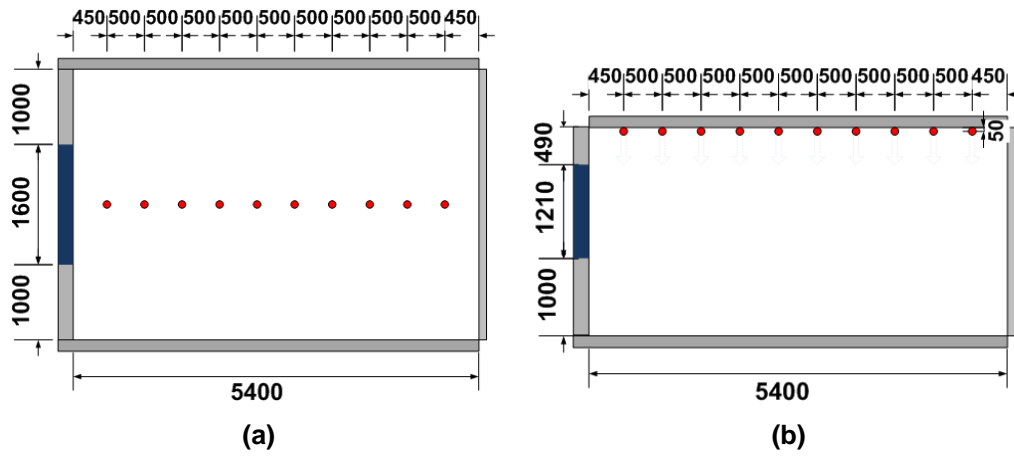


**Fig. 6** (a) Plan view and (b) section view of calculation points for ground contribution

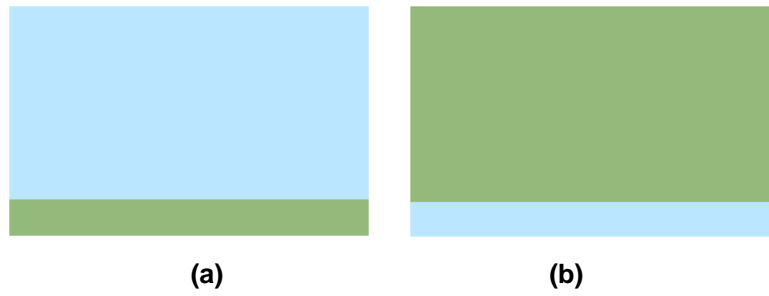
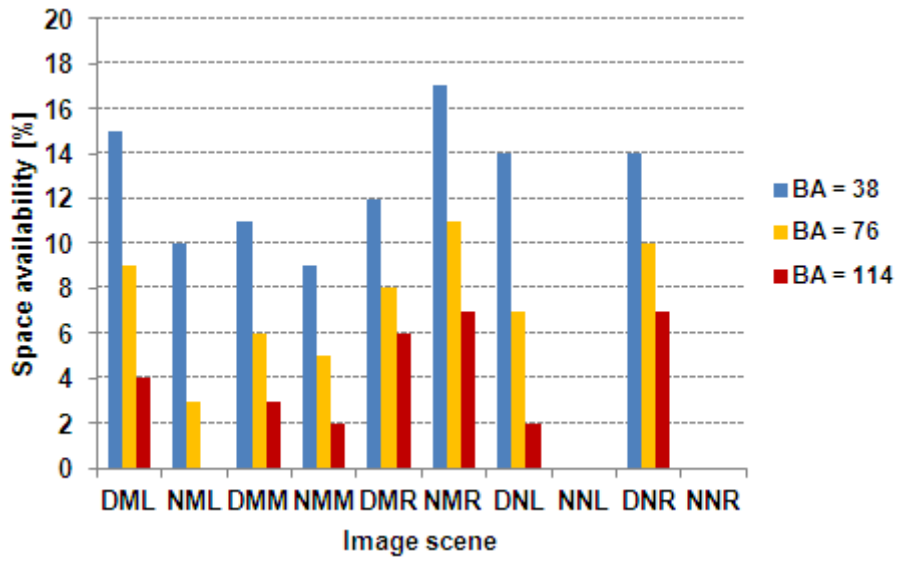
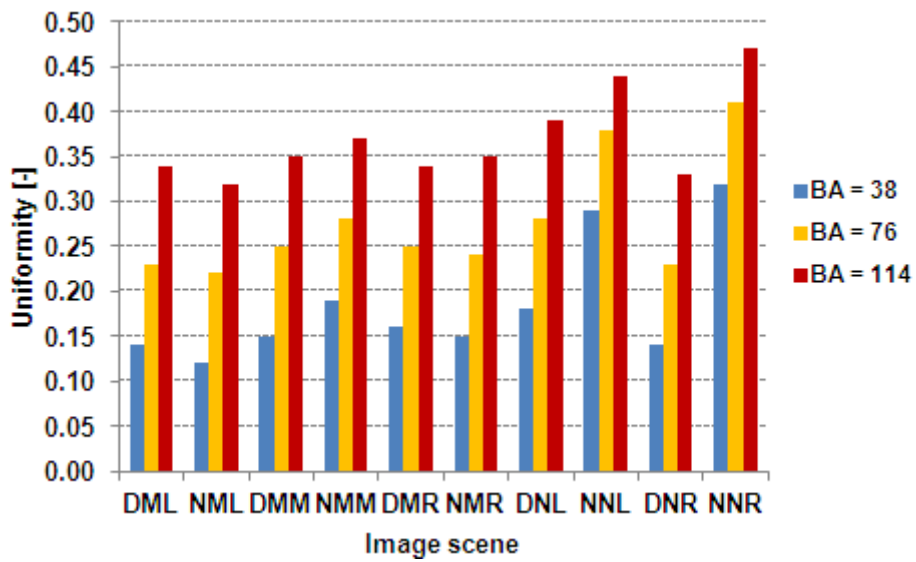


**Fig. 7** Image scenes of (a) 'blue sky and green ground' (BG) and (b) 'green obstructed sky and blue ground' (GB)



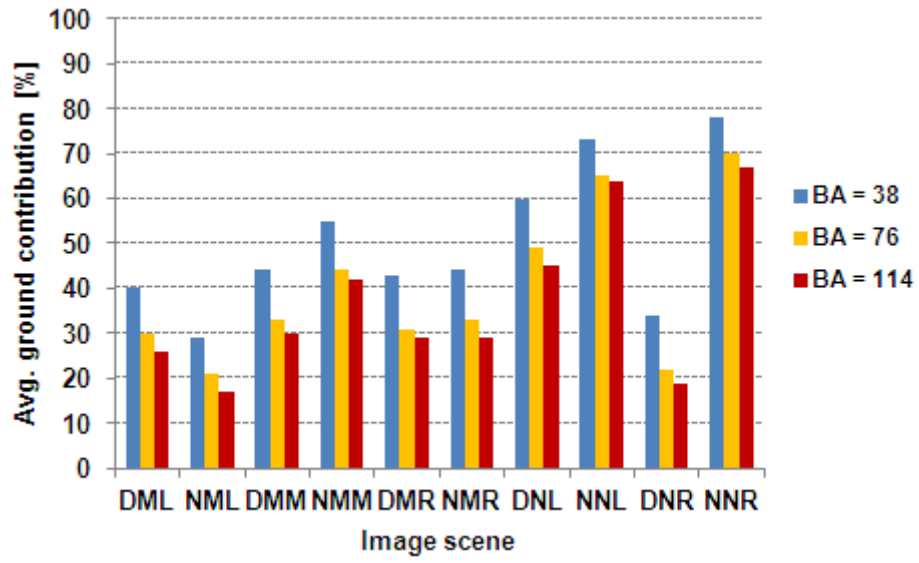
(a)



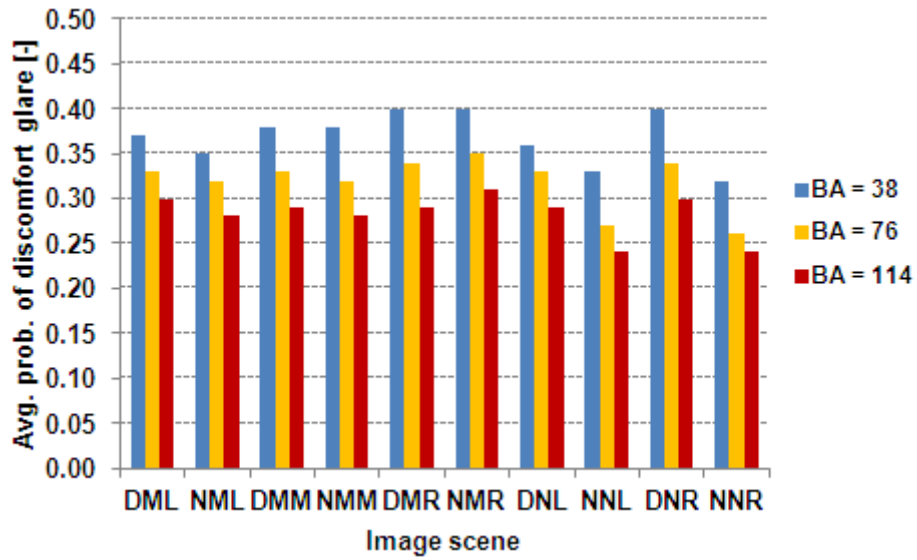
(b)

**Fig. 8** Summary of (a) space availability, (b) uniformity, (c) average ground contribution, and (d) probability of discomfort glare for all variations under the 10 image scenes of VNLS with  $\Phi = 11100$

lm

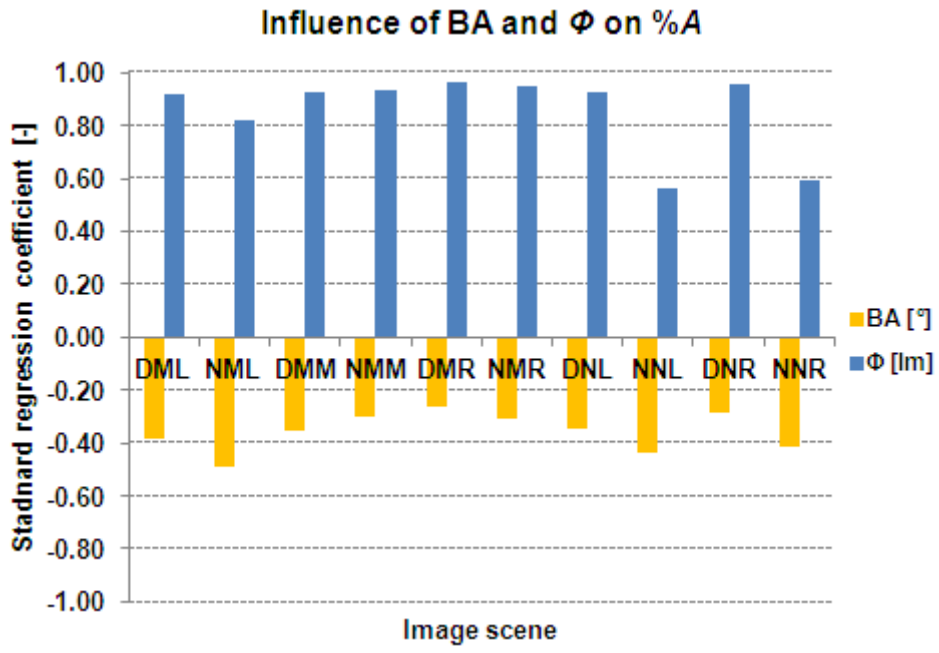


(c)

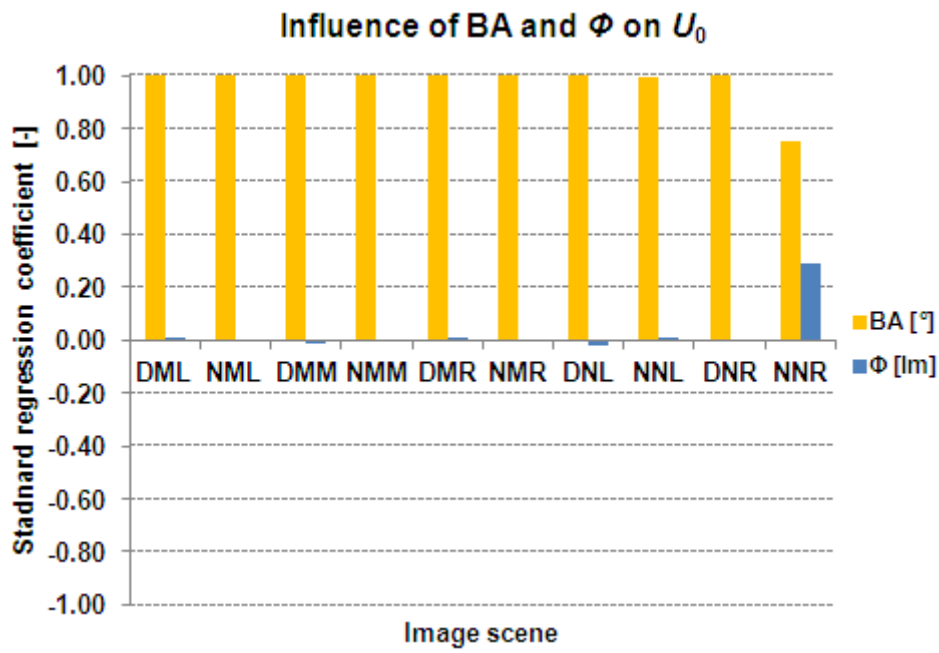


(d)

Fig. 8 (continued)



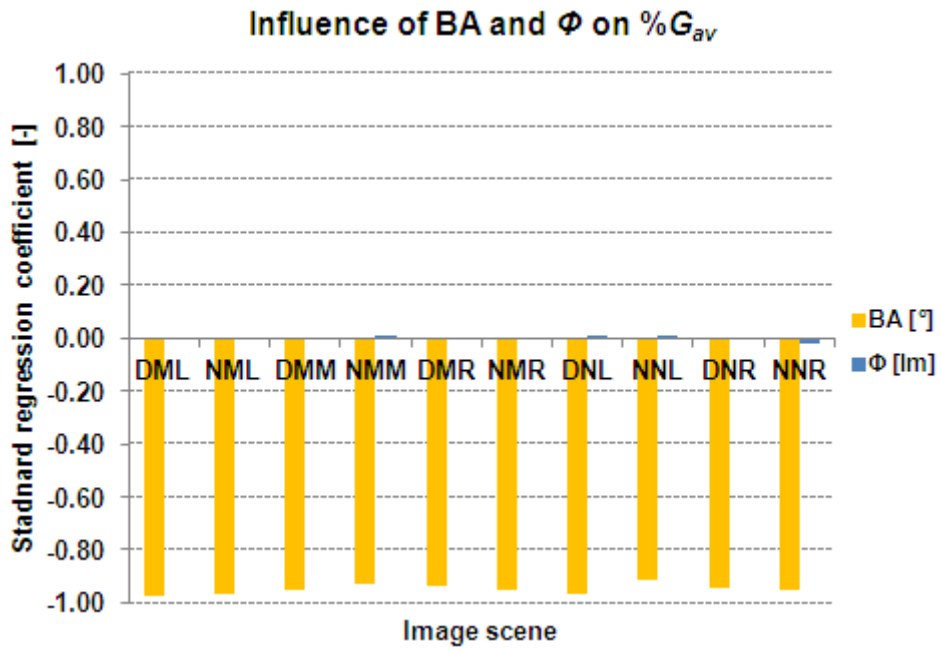
(a)



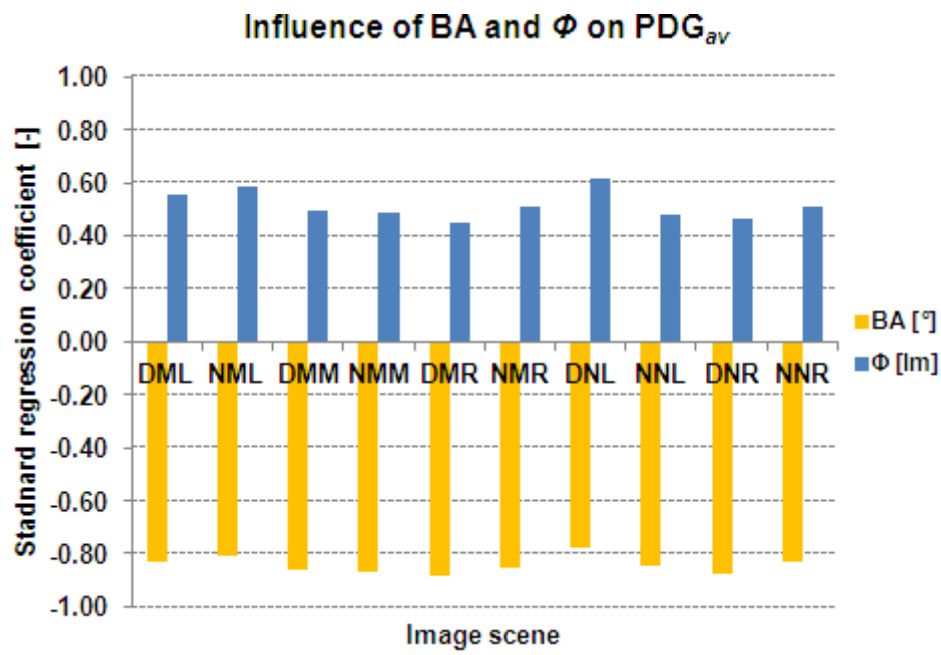
(b)

**Fig. 9** Standard regression coefficient of all input variables (i.e. BA and  $\Phi$ ), evaluated for the four performance indicators, i.e. (a) %A, (b)  $U_0$ , (c) % $G_{av}$ , and (d) PDG $_{av}$  under the 10 image scenes



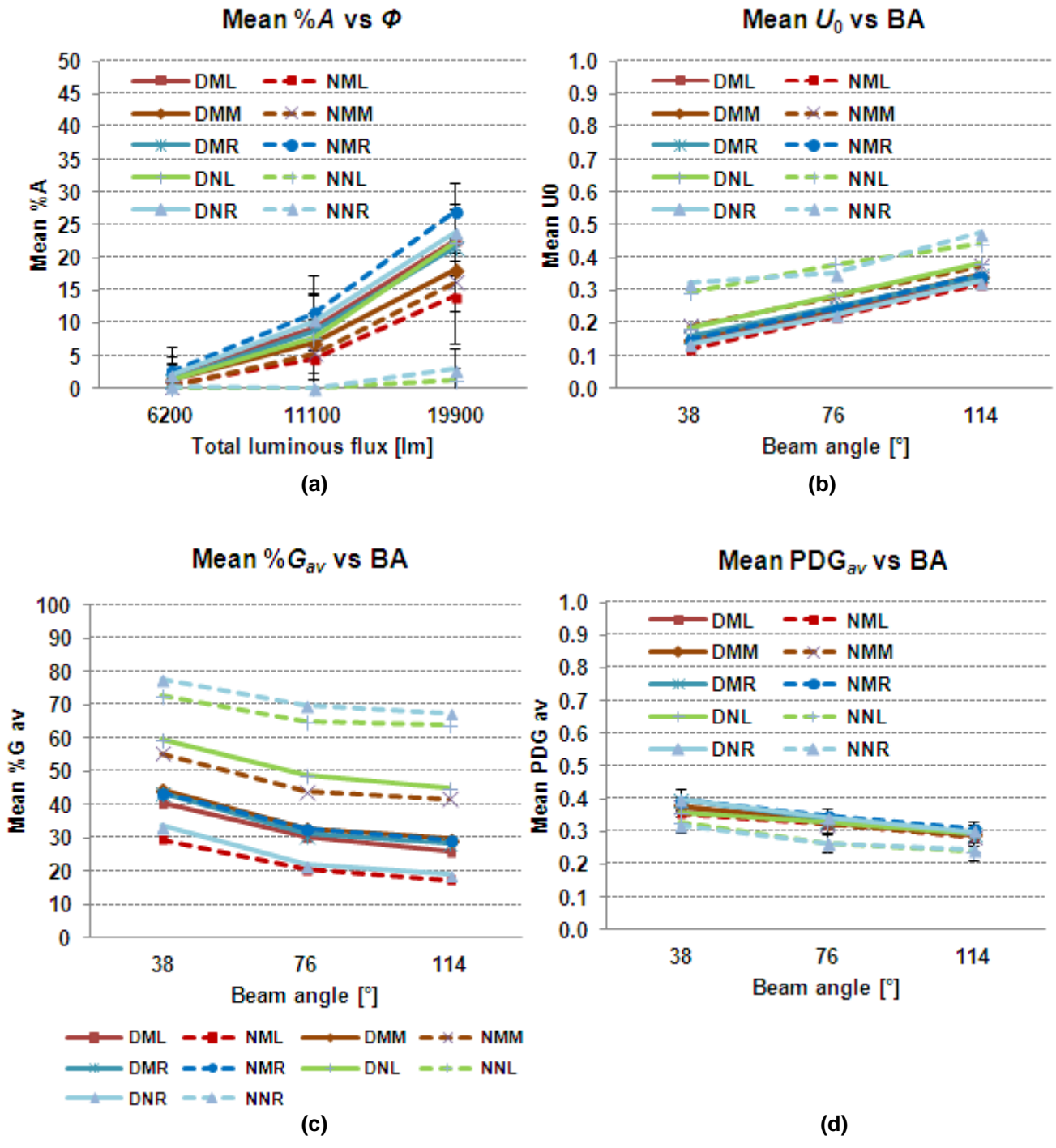


(c)



(d)





Fig. 9 (continued)

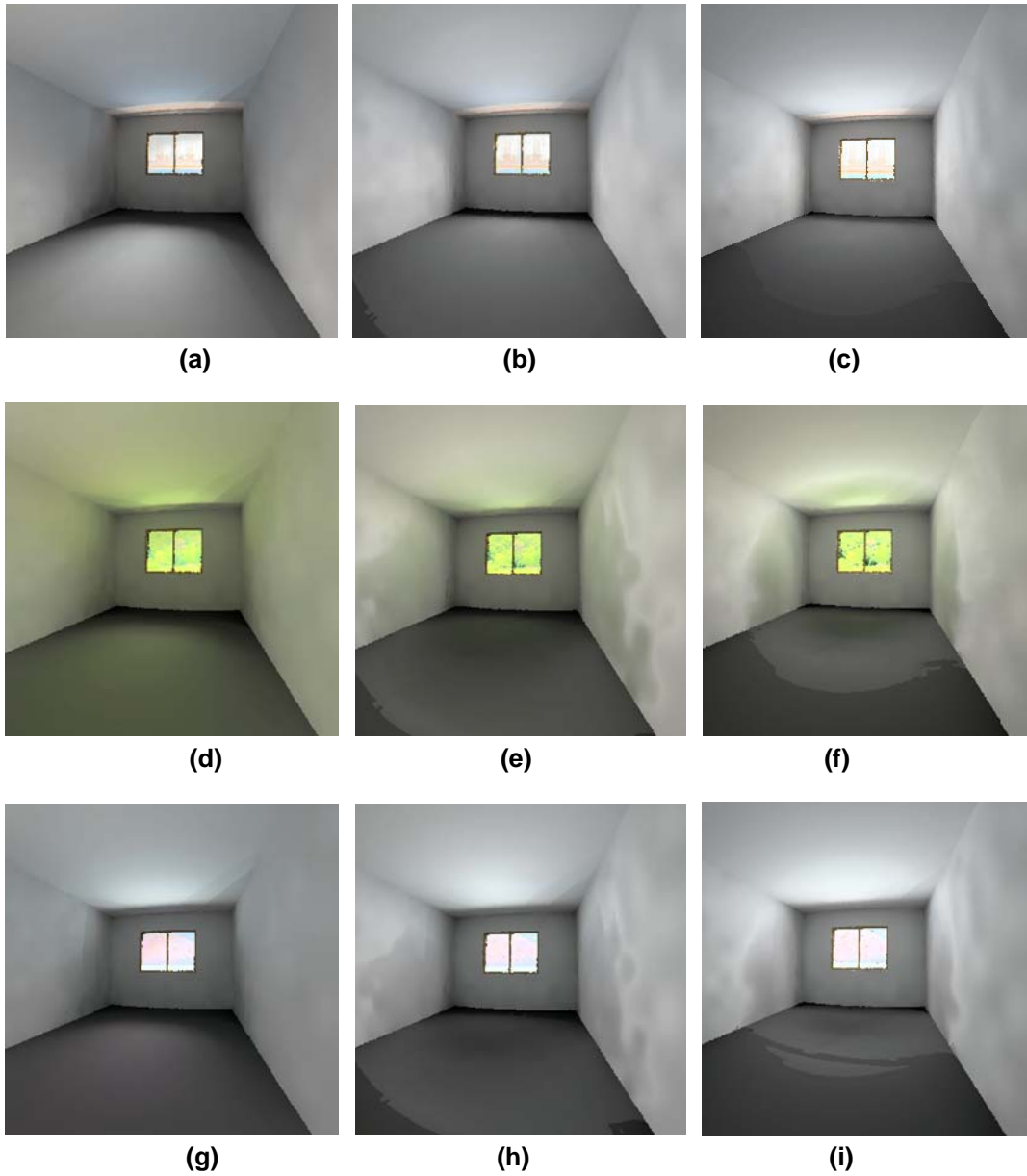


**Fig. 10** Graphs showing the relationship between arithmetic mean of the output (i.e. %A,  $U_0$ , % $G_{av}$ , and  $PDG_{av}$ ) and the most influential input variable(s), with a 95% confidence level



**Fig. 11** Impression of three image scenes, all with  $\Phi = 19900$  lm: (a) NMR, BA = 38°; (b) NMR, BA = 76°; (c) NMR, BA = 114°; (d) NNL, BA = 38°; (e) NNL, BA = 76°; (f) NNL, BA = 114°; (g) NNR, BA = 38° (h) NNR, BA = 76°; (i) NNR, BA = 114°

Scene	Emissive approach	Transmissive approach
BG		
GB		

**Fig. 12** Impression of the BG and GB image scenes with emissive and transmissive approach, all with  $\Phi = 19900 \text{ lm}$  and  $BA = 114^\circ$